Title
Centimeter-Scale and Visible Wavelength Monolayer Light-Emitting Devices

Journal
Advanced Functional Materials, 30(6)

ISSN
1616-301X

Authors
Cho, Joy
Amani, Matin
Lien, Der-Hsien
et al.

Publication Date
2020-02-01

DOI
10.1002/adfm.201907941

Peer reviewed

Centimeter-Scale and Visible Wavelength Monolayer Light-Emitting Devices

Joy Cho[1,2], Matin Amani[1,2], Der-Hsien Lien[1,2], Hyungjin Kim[1,2], Matthew Yeh[1,2], Vivian Wang[1,2], Chaoliang Tan[1,2], and Ali Javey[1,2,]*

[1]Electrical Engineering and Computer Sciences, University of California at Berkeley, Berkeley, CA 94720, United States
[2]Materials Sciences Division, Lawrence Berkeley National Laboratory, Berkeley, CA 94720, United States

*Address correspondence to ajavey@eecs.berkeley.edu

Keywords transition metal dichalcogenide, electroluminescence, WS_2, chemical vapor deposition, monolayer display, visible emission

ABSTRACT

Monolayer two-dimensional transition metal dichalcogenides (TMDCs) have shown great promise for optoelectronic applications due to their direct bandgaps and unique physical properties. In particular, they can possess photoluminescence quantum yields (PL QY) approaching unity at the ultimate thickness limit, making their application in light-emitting devices highly promising. Here we synthesize and characterize large-area WS_2 grown *via* chemical vapor deposition (CVD) for visible (red) light-emitting devices. We perform detailed optical characterization of the synthesized films, which show peak PL QY as high as 12%. Electrically pumped emission from the synthetic WS_2 is achieved utilizing a transient-mode electroluminescence device structure, which consists of a single metal-semiconductor contact and alternating gate fields to

achieve bipolar emission. Utilizing this aforementioned structure, we demonstrate a centimeter-scale (~0.5 cm^2) visible (640 nm) display fabricated using TMDCs to showcase the potential of this material system for display applications.

1. Introduction

Two-dimensional (2D) transition metal dichalcogenides (TMDCs), such as WS_2 and MoS_2, offer versatile layer-dependent properties that have facilitated an emergent field of technological advancements.[1-4] TMDCs scaled down to the monolayer limit are of particular interest, at which point these materials exhibit direct bandgaps and several properties suitable for optoelectronic applications.[5-7] This class of materials does not require lattice-matching to form heterostructures and is amenable to bandgap engineering *via* various methods such as strain.[8-10] Importantly, these materials can exhibit near-unity photoluminescence (PL) quantum yields (QY),[11] even in the presence of defects as long as the particles are kept in the neutral exciton form.[12] PL QY is defined as the ratio of photons emitted to photons absorbed, and is a key figure of merit as it directly dictates the final efficiency when the materials are made into light-emitting devices or photovoltaics. Various micro-scale light-emitting devices have been demonstrated using TMDCs.[13-16] However, a challenge has been the requirement for simultaneous formation of low-resistance contacts to both electrons and holes in the same device. In one specific architecture, we recently demonstrated efficient bipolar carrier injection using transient-mode

operation through a single Schottky contact.[17] The device effectively acts as a light-emitting capacitor, with minimal dependence on the contact metal to the semiconductor. This device structure was shown to work with exfoliated monolayers of MoS_2, WS_2, $MoSe_2$, and WSe_2. Furthermore, large-area (3 mm × 2 mm) emission was demonstrated using WSe_2 monolayers grown by chemical vapor deposition (CVD). Although the WSe_2 devices were bright, their emission is in the near infrared regime (750 nm peak emission). Recently, millimeter-scale WS_2 devices operated in the visible wavelength regime were demonstrated using a vertical architecture with quantum dots and polymers as electron/hole injection layers, but a more efficient device is still demanded.[18] In this regard, we report a centimeter-scale, bright, visible light-emitting device based on WS_2 monolayers synthesized *via* CVD[19-21] using a simple capacitor structure. The CVD-synthesized material exhibits a respectable peak PL QY of approximately 10%, without a droop at high injection levels. Using this material, we fabricate a transient-electroluminescence (t-EL) device and characterize its performance; in particular, its efficient light emission at high injection levels. Finally, we also fabricate a sixteen-pixel display with bright red EL emission (640 nm, peak output power 14 $\mu W\ cm^{-2}$), which is visible in ambient room lighting.

2. Results and Discussion

Figure 1a shows the PL spectra of the synthesized WS_2 measured over a pump dynamic range of 5 orders of magnitude (the inset shows the

normalized PL spectra). The spot-to-spot variation is ~30 meV in peak energy (Figure S1). The corresponding pump-power dependence of PL QY over a pump dynamic range of over 5 orders of magnitude is shown in Figure 1b. Notably, the CVD-grown monolayer does not show a reduction in PL QY at high pump powers.[4] For the case of exfoliated WS_2, a droop is observed at the high pump power regime, which is attributed to biexcitonic recombination.[4,12] The absence of this behavior has been previously observed in CVD-grown WSe_2 and MoS_2;[22,23] however, the underlying mechanism is unknown, although it could be due to differences in background doping or the presence of strain as a result of the growth process.[12,22] Importantly, the lack of droop in the PL QY of CVD WS_2 at high injection levels makes the material a highly attractive candidate for an electroluminescent device.

Growth conditions were optimized in order to maximize the monolayer coverage. Specifically, growth of WS_2 was conducted in a two-heating zone furnace (Figure S2, details in Methods), with growth substrates, WO_3 and KBr loaded into the downstream zone, and sulfur loaded into the upstream zone. The upstream zone temperature, in conjunction with the residual heat from the downstream zone, was used to control the sulfur vapor pressure and consequently the lateral coverage of WS_2. The optical images in **Figure 2**a show that the monolayer coverage increases with the upstream zone temperature (sulfur temperature), with peak coverage achieved at a sulfur temperature of 55 °C. Note that thickness of the film is identified by optical

contrast and confirmed by atomic force microscopy and Raman spectroscopy (Figure S9). At higher sulfur temperatures, the material is predominantly bi/multilayer. The PL QY is within a few percent for all sulfur temperatures (Figure 2b), indicating that changes in coverage do not considerably affect the optical quality, although the samples grown with a sulfur temperature of 55 °C generally show a higher QY. Figure 2c shows centimeter-scale WS_2 monolayer film after optimizing the synthesis conditions, i.e. using a sulfur temperature setpoint of 55 °C. The film exhibits ~90% monolayer coverage across the substrate. The corresponding PL image (Figure 2d) shows uniform emission where the monolayer is present. The dark regions (~10% coverage) in the PL image are attributed to bi/multilayers or pinholes, which could be improved in the future by other growth methods such as metal-organic CVD (MOCVD).

A simple device structure, which we previously used to achieve EL in 2D semiconductors, was utilized here (shown schematically in **Figure 3**a).[17] In short, a single Al electrode (source) is fabricated on the monolayer which is grown directly on a p-doped silicon substrate with a 90 nm thick SiO_2 layer as the gate oxide. The 90 nm oxide layer was selected because it results in a higher extraction efficiency of the emitted light.[24] The device is operated using a bipolar square wave applied to the gate electrode while the source electrode is grounded. While the gate is held at a negative (positive) potential, holes (electrons) accumulate within the WS_2 layer. As the gate voltage (V_g) is switched, holes (electrons) exit the device while electrons

(holes) enter, resulting in the formation of excitons near the contact edge and their subsequent recombination and light emission.[17] It is important to note that the contact material used for the source, as well as the resulting Schottky barrier, are inconsequential to the overall efficiency as the injection during the transient is driven by tunneling through a thinned barrier (the corresponding band diagrams during the operation cycle are shown in Figure S4). Specifically, during the transient, if the voltage polarity is switched very fast (slew rate ~1 V/ns), the voltage does not get dropped across the gate oxide as the semiconductor cannot be charged quickly enough. Instead, the applied voltage is dropped at the metal-semiconductor contact, resulting in a large band-bending within few nanometers of the metal contact. This subsequently results in efficient injection of charge carriers through tunneling, overcoming the problem of Schottky contacts.

For the WS_2 device presented here, the emission extends ~3 µm from the semiconductor contact edge. Due to the operation mechanism described above, injected carriers (*e.g.*, electrons) diffuse inward while the other type of charge (*e.g.*, holes) stored in the steady-state exit the semiconductor through the contact or recombine with incoming carriers. After the V_g transient, before the system reaches steady-state the injected carrier density along the semiconductor is always higher near the source contact than away from the contact. Therefore, the recombination rate is higher near the contact. Note that the emission length depends on the interplay between several parameters, including the radiative lifetime, mobility (for free

carriers), diffusivity (for excitons), and contact barrier height for both type of carriers.

Figure 3b shows a fabricated WS_2 t-EL device. The source contact is patterned as an array of electrodes with a line spacing of 6 μm to maximize the emission area, and the EL measurements are performed in vacuum. When operated, the device shows near-uniform emission over the entire device area (corresponding EL image shown in Figure 3c).[17] The EL emission is in good accordance with the PL emission spectrum of the as-grown material, with minimal differences in peak position and spectral shape (Figure 3d). Device stability was tested by operating the device continuously at a frequency of 800 kHz with a V_g of ±45V for 11.5 hours (Figure 3e). The device continuously emits light throughout the long measurement period, although variation in intensity is observed. The operation mechanism of this device is verified using time-resolved EL (TREL) measurements, as shown in **Figure 4**. Pulsed emission predominantly occurs during negative-to-positive voltage transients and is consistent with the behavior which would be expected from a device with a lower Schottky barrier height to electrons (Figure S5).

To further characterize the transient-mode operation of the device, we investigated the dependence of EL on two primary parameters, specifically frequency and V_g. By operating the device at higher frequencies, the number of transients per second increases and the total light emitted by the device increases proportionally. Under gate frequencies ranging from 1 kHz to 100

kHz, the device shows almost no variation in the emitted photon count per cycle (**Figure 5**a). It should be noted that higher frequency operation was limited by the parasitics in the device and the bandwidth of the power source used to drive the device. The EL as a function of V_g is shown in Figure 5b and indicates that the EL increases linearly with V_g once past the turn-on voltage (V_t) of approximately 15 V (Figure 5b). The V_t is dependent on the bandgap (E_g) of the semiconductor, the gate oxide thickness, and the parasitic impedances in the device. In the future, the onset voltage can be reduced by thinning the gate oxide, with the theoretical lower bound being $V_t \sim E_g/2q$, as discussed in ref 17. A challenge with the extraction of efficiency in t-EL devices is the lack of ability to accurately measure the electron-hole current injection per cycle. However, the overall external efficiency of the device can be roughly approximated as the ratio of emitted photons per cycle to the accumulated electron (n_0) and hole (p_0) concentrations in the device according to:[17]

$$\eta_e = \frac{photons/cycle}{(n_0 + p_0) \times A}$$

where A is the device area. The total carrier concentration injected by the device is given by:[17]

$$(n_0 + p_0) = \frac{C_{ox}(2V_g - E_g/q)}{q}$$

where C_{ox} is the gate oxide capacitance (38.4 nF cm^{-2}) and q is the electron charge. Finally, the external efficiency is converted to an internal value by correcting for the fraction of light which is able to escape from the

semiconductor to free space.[24] The device shows a peak internal efficiency of approximately 4% across the tested frequencies and shows a near-linear increase with respect to V_g (Figure 5c).

To demonstrate the scalability of WS_2 for display applications, we fabricated a centimeter-scale and visible wavelength display utilizing TMDCs. A sixteen-pixel display was directly fabricated on a 7 mm $\times$ 7 mm as-grown WS_2 monolayer (**Figure 6**a). Each pixel is 1.2 mm $\times$ 1.2 mm, consisting of an array of source contacts designed to maximize the contact edge length to capitalize upon emission over the entire pixel area (Figure 6b). The entire display shares a common gate electrode (p++ Si/SiO_2, 90 nm thickness). The device was then packaged in a standard chip carrier in which each pixel was directly wire-bonded, and then measured in vacuum. The pixels show similar performance to the devices shown in Figure 3 and can output a maximum power density of ~14 $\mu W\ cm^{-2}$ at a V_g of ±28 V and frequency of 250 kHz (Figure 6c). Individual pixels can be selectively turned on by grounding the appropriate source contact (Figure 6d). The display was then operated to dynamically display the letters C-A-L under ambient room lighting and recorded using a commercial camera, showcasing the potential for TMDC-based light-emitting displays (Figure 6e-g).

3. Conclusions

In summary, we have demonstrated a centimeter-scale and visible wavelength light-emitting display from CVD-grown WS_2 monolayer

semiconductors. The device operates in the transient mode and exhibits bright red emission, despite the emission layer being only 0.7 nm in thickness. The work highlights the potential use of monolayer semiconductors for ultrathin displays, taking advantage of their high luminescence quantum yields. Future work includes exploration of other monolayer semiconductors and/or strain-engineering for green, blue, and white light emission. Furthermore, the contacts and gate dielectrics can also be scaled down to monolayer or few-layer thicknesses by using appropriate 2D materials, thus enabling the entire device to be at the ultimate thickness limit.

4. Experimental Section

Materials Growth

WS_2 was grown *via* CVD on 90 nm Si/SiO_2 substrates. Growth was done in a two-heating zone furnace (Daepoong Industry, 50602). Substrates were first cleaned in acetone and isopropyl alcohol under sonication, then loaded into the downstream zone. Tungsten oxide (WO_3) and potassium bromide (KBr) were added into an alumina combustion boat (Coorstek) at a 1:1 mass ratio and loaded in front of the substrates. A second alumina boat containing 1 gram of sulfur was placed in the center of the upstream zone. Upon loading, the quartz tube was vacated, and Ar was introduced at 200 sccm, at which the pressure of the setup was adjusted to 10.0 torr. The upstream zone was first ramped to 55 °C, and subsequently the downstream zone to 800 °C. The upstream zone temperature, in conjunction with the residual heat from the downstream zone, was used to control the sulfur vapor pressure and consequently the lateral coverage of WS_2. The optimization results are shown in Figure S6. Once the temperature of the downstream zone was stabilized, Ar flow was lowered to 35 sccm, and H_2 was introduced at 20 sccm. The pressure was lowered to 2.2 torr, and growth was carried out for 22 mins. Upon completion of growth, H_2 flow was stopped and the furnace was opened to rapidly cool down the system.

Device Fabrication

Devices were patterned using conventional photolithographic techniques. However, alkaline developers were found to severely degrade the PL QY of

the material as well as cause spalling of the grown film. Therefore, a tri-layer photolithographic process consisting of MMA EL9 (140 °C, 10 min bake)/ LOR-5A (140 °C, 10 min bake)/ OiR-906 (90 °C, 1 min bake) was used. The photoresist was exposed and developed using an unmodified process, and an additional development step in 50% acetone/50% methanol (by volume) was used to transfer the image to the MMA. Contacts were deposited by thermal evaporation of 40 nm thick Aluminum, and liftoff was performed in room temperature acetone.

Optical and Electrical Characterization

Photoluminescence (PL) and electroluminescence (EL) measurements were conducted using a custom-built micro-PL instrument described in detail in a prior work.[11] All PL and EL measurement signals were passed through a 550 nm dielectric long-pass filter, dispersed by a f = 340 mm spectrometer with a 150 mm g^{-1} grating, and then detected by a Si charge-coupled device (CCD) (Andor iDus BEX2-DD). Prior to each measurement, the CCD background was obtained and subtracted from the resulting acquisition. All measurements were collected via either a 50× (numerical aperture 0.55) or a 10× (numerical aperture 0.25) objective lens. Steady state PL was measured using an Ar^+ laser (Lexel 95) with a 514.5-nm line for excitation. The power density was adjusted *via* neutral filters and monitored by a photodiode power sensor (Thorlabs S120C). External PL QY calibration and the extraction of internal QY was conducted as outlined in our previous study.[11,21] Time-resolved PL was measured using a monochromated 514 nm

line from a pulsed supercontinuum laser (Fianium WhiteLase SC-400) as an excitation source. The resulting signal was detected *via* a single-photon counting avalanche photodiode (ID Quantique) with a time-correlated single-photon counting (TCSPC) module (Becker-Hickl GmbH). Time-resolved EL was measured using an identical collection module. PL and EL imaging were conducted with a fluorescence microscopy setup and a CCD detector (Andor Luca) was used for image acquisition. For PL imaging only, a 470 nm LED excitation source was utilized. For the centimeter-scale film imaging, a CMOS camera with a telephoto lens equipped with a 550-nm colored glass long-pass filter was used. Macroscopic photographs of the EL device was taken with a commercial camera with a single exposure. All EL device measurements were done under vacuum at room temperature. Transistor I_d-V_g characteristics were obtained using an Agilent B1500A semiconductor parameter analyzer (Figure S8).

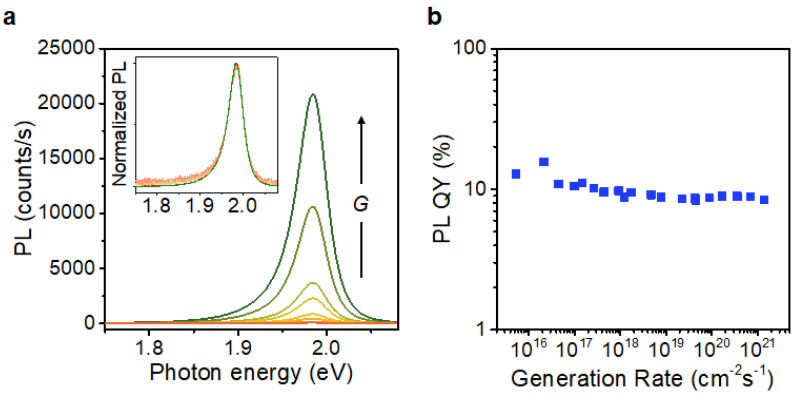

Figure 1. a) The PL spectra of the synthesized WS_2 measured over a pump (*i.e.*, generation rate *G*) dynamic range of 5 orders of magnitude from $G = 10^{16}$ to 10^{21} $cm^{-2}s^{-1}$. The inset is the normalized PL spectra which show a centered emission energy of 1.97 eV. b) The pump power dependence of the PL QY for a typical CVD WS_2 sample.

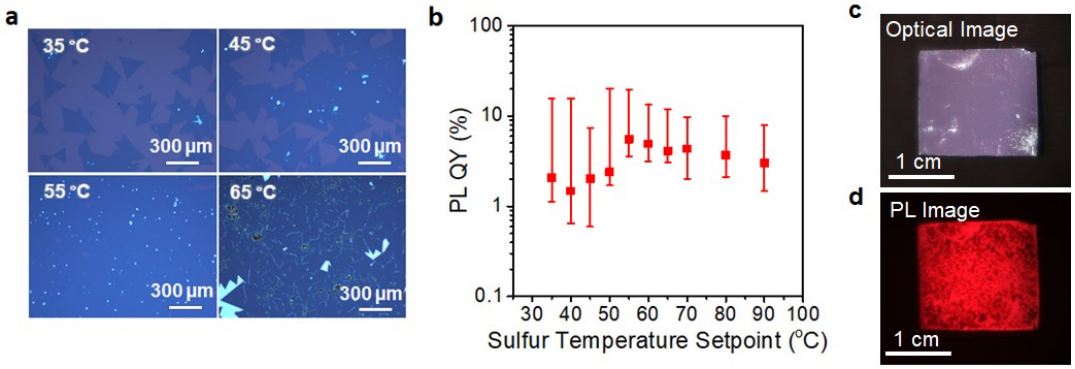

Figure 2. a) Optical microscope images of CVD-grown WS_2 monolayers grown using varying sulfur temperatures. b) PL QY as a function of sulfur temperature. Each error bar shows the maximum, median (dots), and minimum values of the PL QY across 25 random spots on a single sample, for a given temperature. A distribution of PL peak energies is shown in Figure S3. c) Optical image of a CVD-grown WS_2 monolayer film on a 90 nm Si/SiO_2 substrate with a sulfur temperature of 55 °C. d) Macroscopic PL imaging of the CVD-grown sample under excitation by a 470 nm LED.

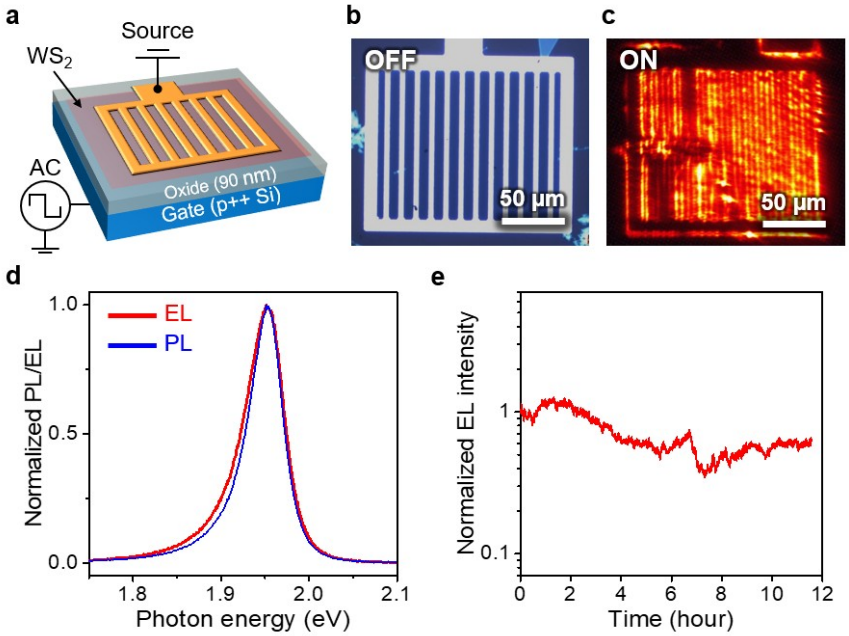

Figure 3. a) Schematic of the t-EL device. b) Optical microscope image of the fabricated t-EL device. c) EL image of the device, showing emission is concentrated near the metal contacts. Taken under V_g = ±28 V and f = 200 kHz. d) PL (at $G = 10^{20}$ $cm^{-2}s^{-1}$) and EL (V_g = ±28 V and f = 200 kHz) spectra of the CVD-grown monolayer WS_2 device. e) Device stability measurement for the t-EL device taken under continuous operation for approximately 12 hours under vacuum.

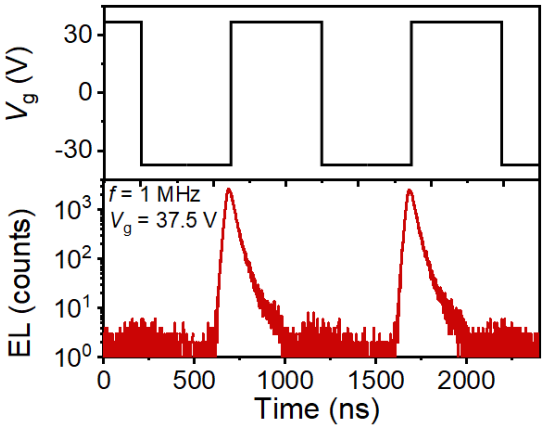

Figure 4. TREL measurement of the WS_2 t-EL device with the corresponding V_g profile shown in the upper panel. Note that the measurement is limited by the slew rate of the amplifier, resulting in a discrepancy between the TRPL (shown in Figure S7) and TREL lifetimes.

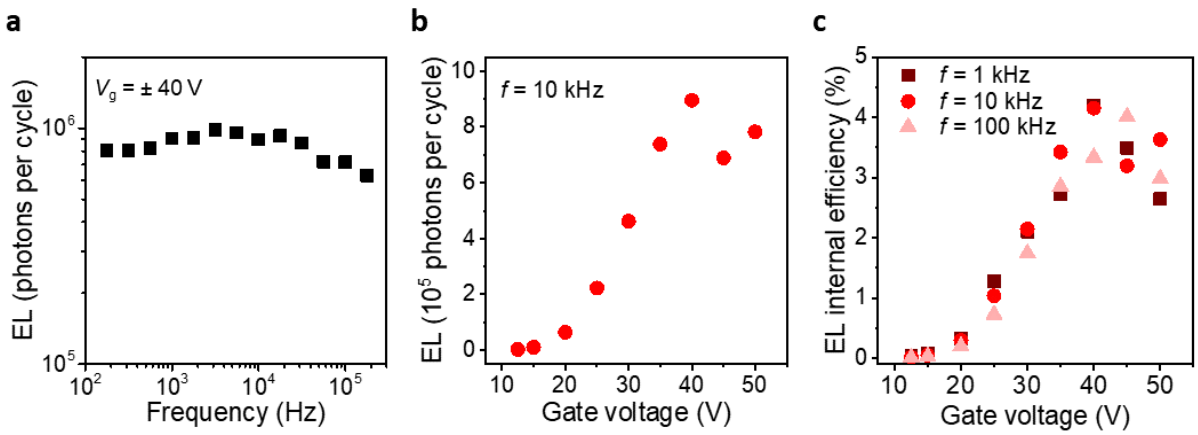

Figure 5. a) Frequency dependence and b) voltage dependence of EL for the CVD-grown WS_2 t-EL device. c) EL internal efficiency of the device as a function of V_g.

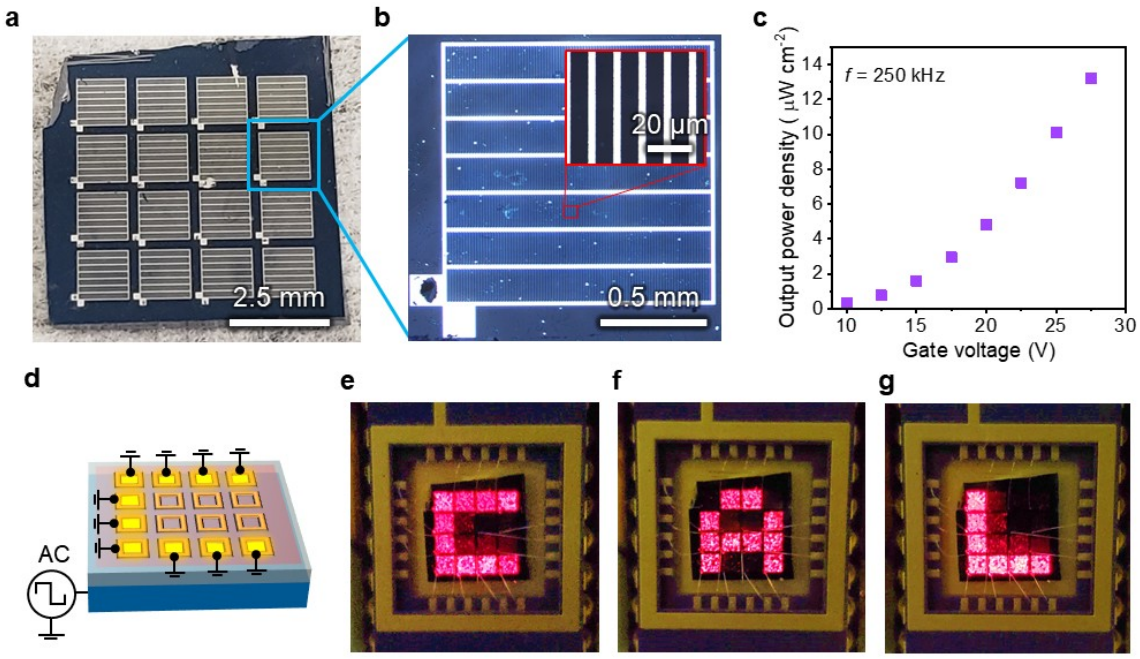

Figure 6. a) Photograph of the sixteen-pixel t-EL display. b) Optical microscope image of an individual pixel. c) Output power density of a single pixel as a function of V_g. d) The operation principle of the sixteen-pixel t-EL display. e-g) Photograph of the device sequentially displaying the letters C-A-L, respectively.

ASSOCIATED CONTENT

Supporting Information

Supporting Information is available from the Wiley Online Library or from the author

Acknowledgements

This work was supported by the Electronic Materials Program, funded by U.S. Department of Energy, Office of Science, Office of Basic Energy Sciences, Materials Sciences and Engineering Division under Contract No. DE-AC02-05Ch11231.

Conflict of Interest

The authors declare no conflict of interest

REFERENCES

[1] F. Xia, H. Wang, D. Xiao, M. Dubey, *Nat. Photon*ics **2014**, *8*, 899-907.

[2] Q. H. Wang, K. Kalantar-Zadeh, A. Kis, J. N. Coleman, M. S. Strano, *Nat. Nano*. **2012**, *7*, 699-712.

[3] A. Splendiani, L. Sun, Y. Zhang, T. Li, J. Kim, C.-Y. Chim, G. Galli, F. Wang, *Nano Lett*. **2010**, *10*, 1271-1275.

[4] M. Amani, P. Taheri, R. Addou, G. H. Ahn, D. Kiriya, D.-H. Lien, J. W. Ager, R. M. Wallace, A. Javey, *Nano Lett.* **2016**, *16*, 2786-2791.

[5] A. Ramasubramaniam, D. Naveh, E. Towe, *Phys. Rev. B* **2011**, *84*, 205325.

[6] H. Zeng, J. Dai, W. Yao, D. Xiao, X. Cui, *Nat. Nano.* **2012**, 7, 490-493.

[7] D. Xiao, G.B. Liu, W. Feng, X. Xu, W. Yao, *Phys. Rev. Lett.* **2012**, *108*, 196802.

[8] H. Fang, C Battaglia, C. Carraro, S. Nemsak, B. Ozdol, J. S. Kang, H. A. Bechtel, S. B. Desai, F. Kronast, A. A. Unal, G. Conti, C. Conlon, G. K. Palsson, M. C. Martin, A. M. Minor, C. S. Fadley, E. Yablonovitch, R. Maboudian, A. Javey., *Proc. Nat. Acad. Sci.* **2014**, *111*, 6198-6202.

[9] G. H. Ahn, M. Amani, H. Rasool, D.-H. Lien, J. P. Mastandrea, J. W. Ager, M. Dubey, D. C. Chrzan, A. M. Minor, A. Javey., *Nat. Comm.* **2017**, *8*, 608.

[10] M. Amani, M. L. Chin, A. L. Mazzoni, R. A. Burke, S. Najmaei, P. M. Ajayan, J. Lou, M. Dubey, *Appl. Phys. Lett.* **2014**, *104*, 203506.

[11] M. Amani, D.-H. Lien, D. Kiriya, J. Xiao, A. Azcatl, J. Noh, S. R. Madhvapathy, R. Addou, S. K. C., M. Dubey, K. Cho, R. M. Wallace, S.-C.

Lee, J.-H. He, J. W. Ager III, X. Zhang, E. Yablonovitch, A. Javey, *Science* **2015**, *350*, 1065–1068.

[12] D.-H. Lien, S. Z. Uddin, M. Yeh, M. Amani, H. Kim, J. W. Ager III, E. Yablonovitch, and A. Javey, *Science* **2019**, *364*, 468-471.

[13] J. S. Ross, P. Klement, A. M. Jones, N. J. Ghimire, J. Yan, D. G. Mandrus, T. Taniguchi, K. Watanabe, K. Kitamura, W. Yao, D. H. Cobden, X. Xu, *Nat. Nano.* **2014**, *9*, 268-272.

[14] B. W. H. Baugher, H. O. H. Churchill, Y. Yang, P. Jarillo-Herrero, *Nat. Nano.* **2014**, *9*, 262-267.

[15] A. Pospischil, M. Furchi, M. T. Mueller, *Nat. Nanotechnol.* **2014**, *9*, 257-26.

[16] F. Withers, O. Del Pozo-Zamudio, A. Mishchenko, A. P. Rooney, A. Gholinia, K. Watanabe, T. Taniguchi, S. J. Haigh, A. K. Geim, A. I. Tartakovskii, K. S. Novoselov, *Nat. Mater.* **2015**, *14*, 301-306.

[17] D.-H. Lien, M. Amani, S. B. Desai, G. H. Ahn, K. Han, J.-H. He, J. W. Ager III, M. C. Wu, A. Javey, *Nat. Comm.* **2018**, *9*, 1229.

[18] D. Andrzejewski, H. Myja, M. Heuken, A. Grundmann, H. Kalisch, A. Vescan, T. Kümmell, G. Bacher, *ACS Photonics* **2019**, *6*, 1832-1839.

[19] H. R. Gutierrez, N. Perea-Lopez, A. L. Elias, A. Berkdemir, B. Wang, R. Lv, F. Lopez-Urias, V. H. Crespi, H. Terrones, and M. Terrones, *Nano Lett* **2013**, *13*, 3447-3454.

[20] S. Najmaei, Z. Liu, W. Zhou, X. Zou, G. Shi, S. Lei, B. I. Yakobson, J.-C. Idrobo, P. M. Ajayan, J. Lou, *Nat. Matter.* **2013**, 12, 754-759.

[21] K. Kang, S. Xie, L. Huang, Y. Han, P. Y. Huang, K. F. Mak, C.-J. Kim, D. Muller, J. Park, *Nature*. **2015**, *520*, 656-660.

[22] H. Kim, G. H. Ahn, J. Cho, M. Amani, J. P. Mastandrea, C. K. Groschner, D.-H. Lien, Y. Zhao, J. W. Ager III, M. C. Scott, D. C. Chrzan, A. Javey, *Sci. Adv.* **2019**, *5*, eaau4728.

[23] M. Amani, R. A. Burke, X. Ji, P. Zhao, D.-H. Lien, P. Taheri, G. H. Ahn, D. Kirya, J. W. Ager III, E. Yablonovitch, J. Kong, M. Dubey, A. Javey., *ACS Nano* **2016**, *10*, 6535-6541.

[24] D.-H. Lien, J. S. Kang, M. Amani, K. Chen, M. Tosun, H.-P. Wang, T. Roy, M. S. Eggleston, M. C. Wu, M. Dubey, S.-C. Lee, J.-H. He, A. Javey, *Nano Letters* **2015**, *15* (2) 1356-1361.

Large-area and visible Wavelength Monolayer Light-Emitting Devices. We demonstrate a centimeter-scale and visible wavelength light-emitting display from CVD-grown WS_2 monolayer semiconductors. The device operates in the transient mode and exhibits bright red emission, despite the emission layer being only 0.7 nm in thickness. The work highlights the potential use of monolayer semiconductors for ultrathin displays, taking advantage of their high luminescence quantum yields.

Joy Cho[1,2], Matin Amani[1,2], Der-Hsien Lien[1,2], Hyungjin Kim[1,2], Matthew Yeh[1,2], Vivian Wang[1,2], Chaoliang Tan[1,2], and Ali Javey[1,2,]*

Centimeter-Scale and Visible Wavelength Monolayer Light-Emitting Devices